Core structure of dislocations in ordered ferromagnetic FeCo

Aleksei Egorov
ICAMS, Ruhr-Universität Bochum, Universitätsstraße 150, 44780 Bochum, Germany and Engineering and Technology Institute (ENTEG), Faculty of Science and Engineering, University of Groningen, Groningen 9747AG, The Netherlands

Antoine Kraych, Matous Mrovec, Ralf Drautz, and Thomas Hammerschmidt
ICAMS, Ruhr-Universität Bochum, Universitätsstraße 150, 44780 Bochum, Germany

(Received 16 February 2024; accepted 1 August 2024; published 11 September 2024)

We elucidated the core structure of screw dislocations in ordered B2 FeCo using a recent magnetic bond-order potential (BOP) [Egorov *et al.*, Phys. Rev. Mater. **7**, 044403 (2023)]. We corroborated that dislocations in B2 FeCo exist in pairs separated by antiphase boundaries. The equilibrium separation is about 50 Å, which demands large-scale atomistic simulations—inaccessible for density functional theory but attainable with BOP. We performed atomistic simulations of these separated dislocations with BOP and predicted that they reside in degenerate core structures. Additionally, dislocations induce changes in the local electronic structure and magnetic moments.

DOI: 10.1103/PhysRevMaterials.8.093604

I. INTRODUCTION

Iron-cobalt combines excellent magnetic properties and severe brittleness [1]. The latter can be related to how the atoms arrange in a compact region surrounding the dislocation line—the dislocation core [2]. Although many experimental [3–6], theoretical [7,8], and computational [9–12] studies have examined the mechanical properties of ordered Fe-Co alloys, the dislocation core structure remains unknown. Observing cores experimentally proves complicated [13–15], and quantum mechanical calculations based on density functional theory (DFT) [16,17] face difficulties due to the large simulation cells required for modeling ordered alloys with dissociated dislocations [18].

Dislocations carry plastic deformation [19]. If a crystal deforms easily, dislocations must be mobile under low applied stress. When immobile, they cannot relieve stresses by shearing the crystal; cracks start to grow and material fractures [20]. In metals with the body-centered cubic (bcc) structure, $\frac{1}{2}$[111] screw dislocations govern low-temperature plasticity due to their compact, non-planar core structure [21–24]. Their core structures can be divided according to symmetry into degenerate and nondegenerate (see Fig. 1). DFT studies revealed that the nondegenerate core is the ground state for pure bcc metals [25–29]. Degenerate cores, for a long time, remained just the artifacts produced by classical potentials [30], until Romaner *et al*. observed degenerate cores with DFT in disordered bcc alloys, first in W-Re [31] and then in Fe-Co [32]. The authors also speculated that the degenerate core exists in ordered B2 (CsCl) FeCo (the most stable phase at 1:1 composition [33]) but exploring it with DFT was not feasible.

The behavior of screw dislocations in ordered and disordered Fe-Co alloys is distinctly different. In tensile tests, the ordered B2 FeCo fractures in a brittle manner without elongation, whereas the disordered FeCo before fracture displays some ductility [5]. In the latter, wavy dislocation slip lines [4] indicate profuse cross-slip, similar to pure bcc transition metals. This similarity implies that in disordered FeCo, ordinary $\frac{1}{2}$[111] screw dislocations govern plasticity. In contrast, in (partially) ordered B2 FeCo, the straight slip lines indicate rare cross-slip. This behavior likely arises from disparate dislocations presented in B2 FeCo. When an ordinary $\frac{1}{2}$[111] screw dislocation glides in a B2 crystal, it disrupts the chemical order within the {110} slip plane, producing an interface known as antiphase boundary (APB). Therefore, plasticity in B2 alloys is governed by so-called superdislocations [18,23], with Burgers vectors two times larger than those of ordinary ones. Superdislocation gliding through B2 crystal retains its chemical order.

In B2 FeCo, [111] screw superdislocations dissociate into two ordinary $\frac{1}{2}$[111] screw dislocations, called *partial dislocations* or *partials*, separated by an APB, which glide together (Fig. 2) [4,36]. The equilibrium separation depends on the balance of two opposing forces: the elastic repulsion of the partials with the same Burgers vector counters the tension due to the energy cost of creating APB between them [37]. The estimated separation of the partials in B2 FeCo is about 50 Å [38], and their modeling would entail simulation cells with thousands of atoms—unfeasible for DFT [39]. Classical interatomic potentials, such as the embedded-atom method (EAM) [40] and the modified EAM (MEAM) [41–43], easily handle large simulation cells but only crudely describe the angular character of the bonding, vital for bcc transition metals [44,45]. This renders EAM and MEAM ambiguous for core structures [30]. Besides, these potentials usually lack magnetism (and magnetism is the fulcrum of the Fe-Co properties [46–48]). Machine learning (ML) interatomic potentials combine exceptional accuracy and efficiency [49–53] and already

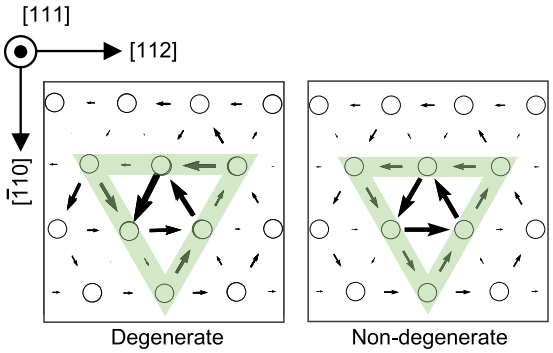

FIG. 1. Differential displacement illustrates the two possible core symmetries of the $\frac{1}{2}$[111] screw dislocations in bcc-like crystals—B2 FeCo (left) and bcc Fe (right) obtained with BOP [34]. The arrows reveal the changes in atomic positions along the [111] direction of the dislocation line compared to a bulk defect-free cell. On the left, longer and shorter arrows alternating on a green triangle reveal the degenerate core. Conversely, on the right, the same length of the arrows reveals the nondegenerate core [35].

showcased their aptness for dislocation cores in bcc metals [54–60]. However, they require extensive DFT reference data [49,50,52,53], and magnetic ML potentials are nascent [58,61–66].

Bond order potentials (BOPs) are interatomic potentials based on a tight-binding model [67,68]. They suffice modeling systems with tens of thousands of atoms and, in addition, treat magnetism explicitly. BOPs proved their aptness for many transition metals [69–73] and, specifically, for $\frac{1}{2}$[111] screw dislocations in W [74], Mo [75], and Fe [76]. The core structures match DFT results in every case, evincing BOPs' reliability for dislocations.

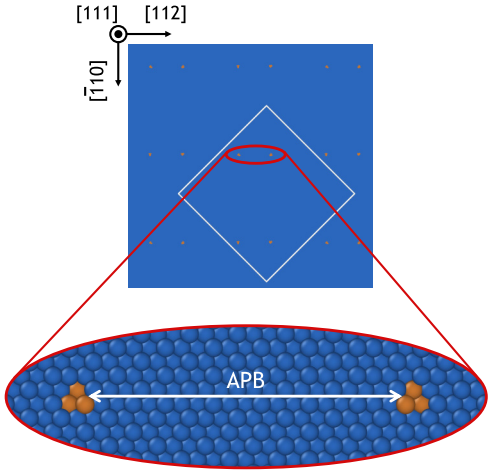

FIG. 2. 15048-atom periodic simulation cell (white square) for the core structure of partial dislocations in B2 FeCo. Two pairs of partial $\frac{1}{2}$[111] screw dislocations in {110} plane were introduced into the cell, resulting in their quadrupolar arrangement. The blue atoms are the bulk B2, and the orange is the dislocation cores [94]. Partials are separated by an antiphase boundary (APB) where the B2 order is distorted. The thickness of the cell is $2 \times \frac{1}{2}$[111] or 4.93 Å.

We recently developed an accurate and transferable magnetic BOP for Fe-Co alloys based on DFT reference data [34]. Here, we employed it for large-scale atomistic simulations of screw dislocations in ordered ferromagnetic B2 FeCo. First, to vindicate BOP's validity for dislocations, we tested how accurately it predicts the γ surface of the slip plane. We then assessed the partial dislocations' equilibrium separation and elucidated their cores' symmetry. We also examined how local magnetic moments and electronic structure change in the cores.

II. SIMULATION DETAILS

A. Computational details

We used the VASP package [77–79] for DFT calculations with the projector augmented wave (PAW) method for pseudopotentials [80], PBE (Perdew-Burke-Ernzerhof) exchange-correlation functional [81], 400 eV cut-off energy, and dense Monkhorst-Pack k-point meshes [82]. We used the BOPFOX package [83] for analytic BOP calculations with the same settings as in Ref. [34] and employed the LAMMPS [84] package implemented in the Atomic Simulation Environment (ASE) [85] for MEAM. Atomic positions were relaxed using the FIRE algorithm [86] until forces were less than 0.03 eV/Å for the γ surface calculations and 0.003 eV/Å for the core structures. We used a weaker convergence criterion for the γ surfaces to speed up DFT calculations while fast-computing BOP allowed us to use a tighter convergence criterion for the core structures.

B. Setup for computing the γ surface

To compute the γ surface for a slip plane we adopted a periodic simulation cell, cut it in half on a {110} plane, displaced one part of the bicrystal with respect to the other half in all directions, and calculated the energy as a function of the displacement. The energy difference with respect to a bulk crystal, divided by the area of the cut plane, is the generalized stacking fault energy (GSFE) [87]. In all calculations, we relaxed the positions of atoms in the direction perpendicular to the cut plane only, as relaxation in other directions would annihilate the stacking fault [74,75,87]. For the γ surfaces, we computed energies on a 9×9 grid; the discrete values of the energies were then converted into smooth contour plots through extrapolation (Fig. 3).

C. Setup for dislocation core structures

To clarify if and how the [111] screw superdislocations dissociate, we adopted a periodic cell containing two superdislocations with opposite Burgers vectors, resulting in their quadrupolar arrangement (see Fig. 1 in the Supplemental Material [88]) [39,89,90]. To analyze the core structure of partials, we replaced every [111] screw superdislocation with a pair of ordinary $\frac{1}{2}$[111] screw dislocations at a distance, retaining the same quadrupolar arrangement (see Fig. 2). Dislocations were introduced into the simulation cell by displacing atoms according to isotropic elasticity theory using the BABEL package [91]. A homogeneous strain is applied to the simulation cell to level out the strain caused by the

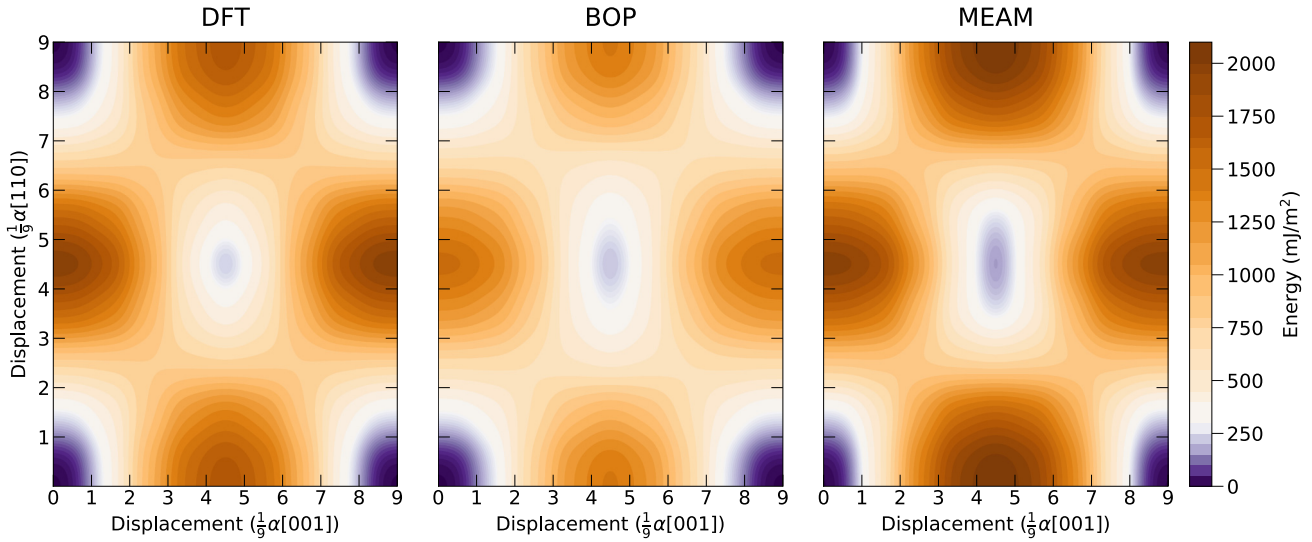

FIG. 3. Relaxed γ surfaces for the {110} plane (experimental slip plane [95]) in B2 FeCo. Diagonals on these plots are the [111] direction—experimental slip direction [95]. Local minima at the middle correspond to an antiphase boundary (APB) with distorted B2 order obtained when we shift two crystal parts concerning each other by $\frac{1}{2}a$[111] (a is a lattice parameter).

introduced dislocations [39,92,93]. To get the equilibrium configurations, we relaxed all atomic positions. The thickness of the simulation cell is a[111], equal to the Burgers vector of the superdislocation. To reduce dislocation-dislocation interactions, we tested the convergence by varying cell sizes in the directions perpendicular to the dislocation line. The resulting $132.39 \times 132.76 \times 4.93$ Å simulation cell contained 15048 atoms (white square in Fig. 2). For an illustrative example of the core structure in bcc Fe (Fig. 1), we used a 135-atom simulation cell with a quadrupolar dislocations arrangement (see Fig. S1a in Ref. [93]).

III. RESULTS AND DISCUSSION

A. γ surfaces

We first evaluated the γ surfaces, which portray the lattice resistance against slip for a given plane. A BOP γ surface matching the DFT would vindicate the BOP efficacy for dislocations because interatomic potentials, which produce accurate γ surfaces, are usually also accurate for core structures [53]. The DFT reference data for this BOP lacked the γ surfaces [34]; thus, verifying if the BOP could predict them accurately was crucial. We obtained the relaxed γ surfaces for the {110} plane—the preferable slip plane [95]—with BOP, DFT, and MEAM [96]. All three produce similar γ surfaces (Fig. 3), with a local minimum at the center corresponding to the antiphase boundary (APB). A single minimum indicates that the superdislocation dissociates into two partials with $\frac{1}{2}a$[111] Burgers vectors [97], precisely what most studies have assumed for B2 FeCo [4].

In bcc metals and alloys, the curvature of the γ surface contour lines hints at the symmetry of the dislocation cores. Circular contour lines between two minima along [111] direction lead to nondegenerate cores; conversely, the contour lines deviating from a circular lead to degenerate cores (see, for example, Fig. 2 in Ref. [31] or Fig. 1 in Ref. [98]). For all three cases in Fig. 3, the contour lines crossing the [111] direction deviate from a perfect circular shape, hinting at degenerate cores in B2 FeCo.

Also, obtaining an accurate equilibrium separation between partial dislocations relies heavily on the accurate APB energies (local minima at the middle), and, for BOP and DFT, they are close (see Table I). The MEAM predicts far lower APB energy, conceivably due to a lack of magnetism. Excess energy after the $\frac{1}{2}$[111] shift in the {110} planes could result from an improper B2 order of two constituent chemical species but also from the disturbed magnetic order alone,

TABLE I. Separation of the partial $\frac{1}{2}$[111] screw dislocations in B2 FeCo, d_{APB}, (i) from isotropic elasticity theory (elastic) with input data required for calculation: equilibrium lattice parameters, a, Voigt-Reuss-Hill shear modulus, G_{VRH} [103], and antiphase boundary (APB) energy, γ_{APB}, for {110} and {211} planes and (ii) separation from atomistic simulations (details on Fig. 4).

	a (Å)	G_{VRH} (GPa)	$\gamma_{\mathrm{APB}_{\{110\}/\{211\}}}$ (mJ/m^2)	d_{APB}, (Å)	
				Elastic	Atomistic
BOP[a]	2.845	73	132/152	53	49
DFT[a]	2.844	93	114/171	79	
DFT[b]	2.843	91			
DFT[c]			129/169		
MEAM[d]	2.859	83	70/81	116	
Exp.	2.857[e]	72[e]	157[f]	45	

[a]This work.
[b]Reference [104].
[c]Reference [105].
[d]Reference [96].
[e]Reference [106], measured at 293 K.
[f]Reference [38].

like in antiferromagnetic bcc Cr [99,100]. A marked increase of the APB energy due to magnetism was also observed in ordered $L1_2$ Ni_3Al [101]. Thus, we surmise that considering magnetism in our study is vindicated.

We also computed APB energy for {211} planes. Compared to {110}, it is about 20–30% higher. This difference entices the partials to dissociate in the {110} plane. For the {211} plane, BOP again closely matches a DFT ABP energy, while MEAM yields a far lower value (see Table I).

To summarize, the BOP predictions above align with DFT, both for the topology of the γ surface and for the APB energies, which instills confidence that this BOP is well suited for studying dislocations in B2 FeCo.

B. Equilibrium separation of the partials

To dissect the cores of the partial dislocations in B2 FeCo, we first need to know how far apart they are. Isotropic elasticity theory can roughly estimate the equilibrium separation from the balance between partial dislocations elastic repulsion and the APB energy (see Eq. A7 in Ref. [102]). The elastic equilibrium separation (Table I) we calculated with BOP input (53 Å) is lower than with DFT input (79 Å) due to the lower shear modulus, which, along with APB energy, defines the separation (see Eq. A7 in Ref. [102]). Nevertheless, the BOP result is close to 45 Å calculated with experimental input (though serendipitously because BOP shear modulus and APB energy, which are proximate to experimental ones, were not in the reference data for this BOP [34], and their values are predictions). The low APB energy obtained with MEAM yields a too-large separation of 116 Å, close to an experimental 125 Å for partially ordered FeCo with long-range order parameter $S = 0.59$ [4].

In the atomistic simulations with BOP (at 0 K), [111] superdislocations do not dissociate unless the atomic positions are randomly distorted. Then, BOP correctly predicted that during relaxation, every [111] superdislocation dissociates into two $\frac{1}{2}$[111] partials connected by APB. Random distortions led partials astray, and they could move both on {110} and {211} planes, depending on the distortion (see additional details in Supplemental Material [88]). Undistorted superdislocation stays undissociated because, at 0 K, partials cannot surmount a Peierls barrier. Therefore, we varied distances between partials on {110} plane and, again, after relaxation, evaluated the cell's relative energies (Fig. 4). The curve attains equilibrium separation at 49 Å, with energy much lower than that of undissociated superdislocation (or any randomly distorted dissociated configuration), manifesting that it is the ground state. Furthermore, the equilibrium separation agrees closely with the elasticity theory (cf. Table I). The slight difference between the elastic and atomistic separations may be attributed to the finite size of the cores, atomic interactions, or anisotropic effects.

C. Dislocation core structures

Employing the equilibrium separation of the partial dislocations (d_{APB} in Fig. 4), we obtained their relaxed cores with BOP. We then scrutinized the core structures with a differential displacement map [109] and the screw component

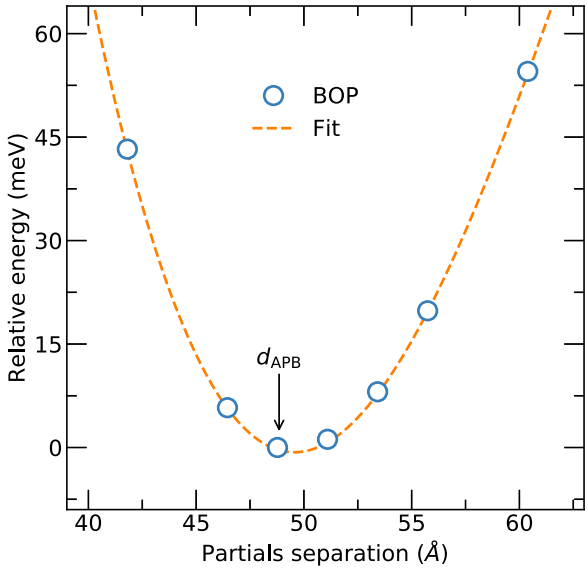

FIG. 4. Relative energy of the simulation cell versus separation of the partial dislocations obtained using BOP. The minimum corresponds to the equilibrium separation of the partial dislocations, d_{APB} (see also Table I).

(α_{33}) of the Nye tensor [110], which portrays the continuous distribution of the Burgers vector [14,111,112]. We revealed that both cores attain distorted degenerate structures spread predominantly along the APB fault [Fig. 5(a)]. Romaner *et al.* with DFT obtained similar cores for individual $\frac{1}{2}$[111] screw dislocations in disordered bcc Fe-Co [32]. The authors also observed a change from the nondegenerate core at low Co concentrations, starting from zero, that is, from pure Fe to the degenerate core at around 1:1 composition (it is worth noting that, for pure Fe, our BOP also correctly predicts the nondegenerate core; see Fig. 1).

Core symmetry in bcc-like Fe-Co alloys may differ from the one in pure Fe, with its nondegenerate core, due to pure Co being hcp. Bcc alloys, where both constituents reside in a bcc ground state, such as W-Mo or W-Ta, retain nondegenerate cores [113,114]. However, if one constituent resides in another ground state (as in W-Re, where pure Re is hcp), the degenerate core structure seems preferable [31,115]. We confirmed the same here.

Additionally, in a recent work, Wang *et al.* linked the core structure in bcc metals and alloys to the energy differences between their bcc and fcc phases, expressed in the materials index χ [116]. χ emanates from the bcc-fcc energy difference in the pure bcc metal (in our case, Fe) and the same in the alloy (in our case, the energy difference between bcc-based B2 and fcc-based $L1_0$ phases in FeCo). These differences computed with BOP closely match the DFT values [34]. A resulting χ index of roughly 0.69 corresponds to the degenerate core structure (near the transition from nondegenerate) [116], which is what we observed in B2 FeCo.

As magnetism defines the Fe-Co phase stability [47,48], we also looked at how the local magnetic moments change in the dislocation cores. In disordered bcc Fe-Co, as Romaner

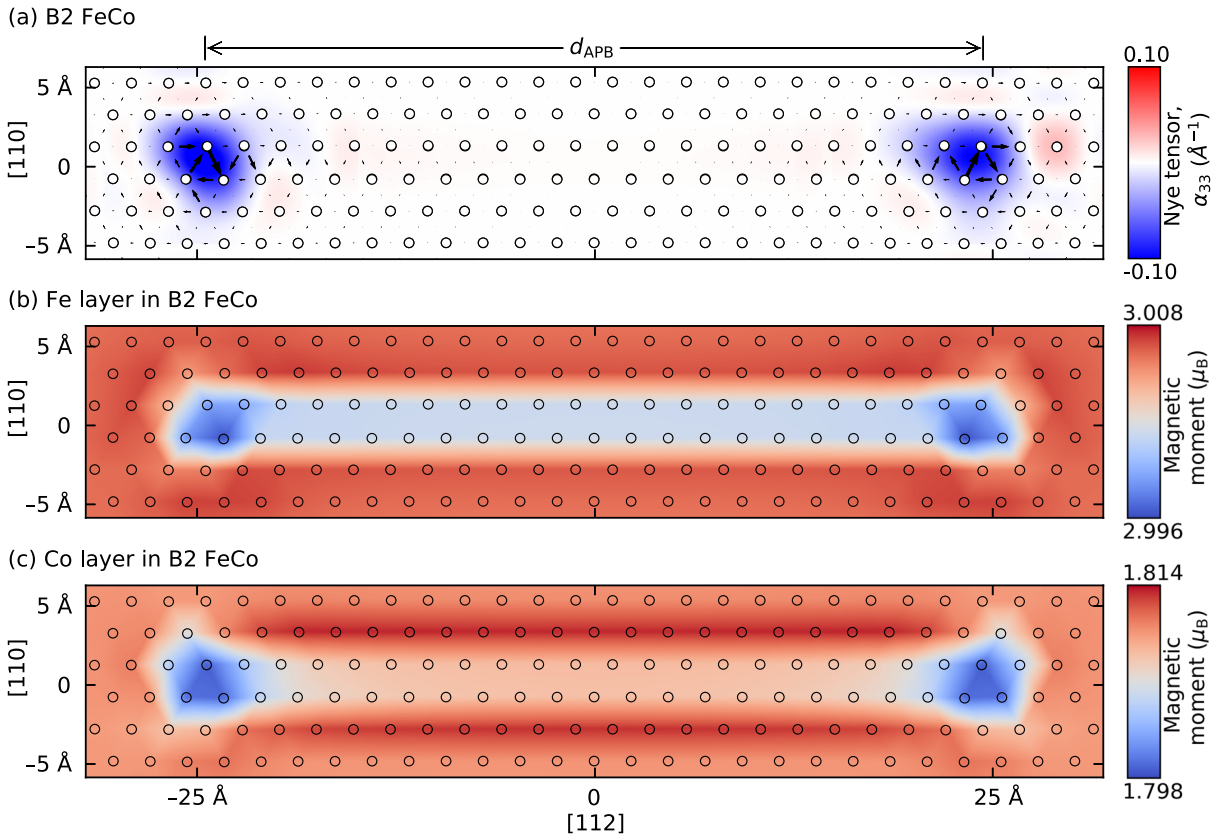

FIG. 5. The core structure of partial $\frac{1}{2}$[111] screw dislocations in B2 FeCo we obtained with BOP [107]. Partials separated by an antiphase boundary (APB) of the length $d_{APB} = 49$ Å (See Sec. III B). The differential displacement and Nye tensor distribution (a) reveal degenerate core structures [108]. Additionally, the local magnetic moments of Fe and Co layers in B2 FeCo [(b) and (c)] display lower magnetic moments within the cores and APB, compared to bulk.

et al. observed with DFT, they decrease [32]. The authors linked it to the *d*-band filling, and we can expect the same due to a similar band filling in B2 FeCo [117]. Indeed, we observed that the magnetic moments of both Fe and Co atoms in the core decreased [Figs. 5(b) and 5(c)]—moreover, the decrease within 1% correlates with the decrease in bcc Fe-Co [32]. (Tight-binding-based methods, such as BOP, provide reliable energy differences between competing magnetic and nonmagnetic phases, but the exact values of magnetic moments are not always robust [118]. Thus, we should approach magnetic moment predictions with a grain of salt; even DFT calculations with different exchange-correlation functionals render different results for magnetic moments in the core [27,32,119–121].)

We also examined how dislocations modify the electronic structure, namely, the local density of states (DOS) of the atoms in the cores. For the bulk B2, BOP predicts magnetic and nonmagnetic DOS, which is consistent with DFT (see Fig. 3 in Ref. [34]); thus, we can rely on the BOP predictions. For the local DOS in the dislocation core, we observed moderate changes for the Fe atoms and distinct for the Co atoms (Fig. 6). For Co, some lower energy states (for spin down) shift closer to the Fermi level compared to the bulk B2, thus increasing the band energy. As Dezerald *et al.* unraveled, such an increase affects the core energies and the Peierls energies of dislocations in bcc transition metals, increasing them too [28]. We can expect similar dependency in transition metal alloys, including B2 FeCo. (We will present the Peierls energy for the B2 FeCo and compare it with those in disordered FeCo and pure Fe in a separate publication.)

IV. SUMMARY AND CONCLUSIONS

Using a magnetic bond-order potential (BOP), we determined the atomic core structure of $\frac{1}{2}$[111] screw dislocations in ordered B2 FeCo and can draw the following main conclusions:

(i) The γ surface for the {110} slip plane obtained using BOP is consistent with DFT.

(ii) Screw dislocations in B2 FeCo exist in pairs, separated by a 50 Å wide antiphase boundary. This large separation obstructs DFT simulations while it is reachable for BOP.

(iii) $\frac{1}{2}$[111] screw dislocations in B2 FeCo—unlike most bcc transition metals but likewise disordered FeCo [32]—accommodate degenerate core structures.

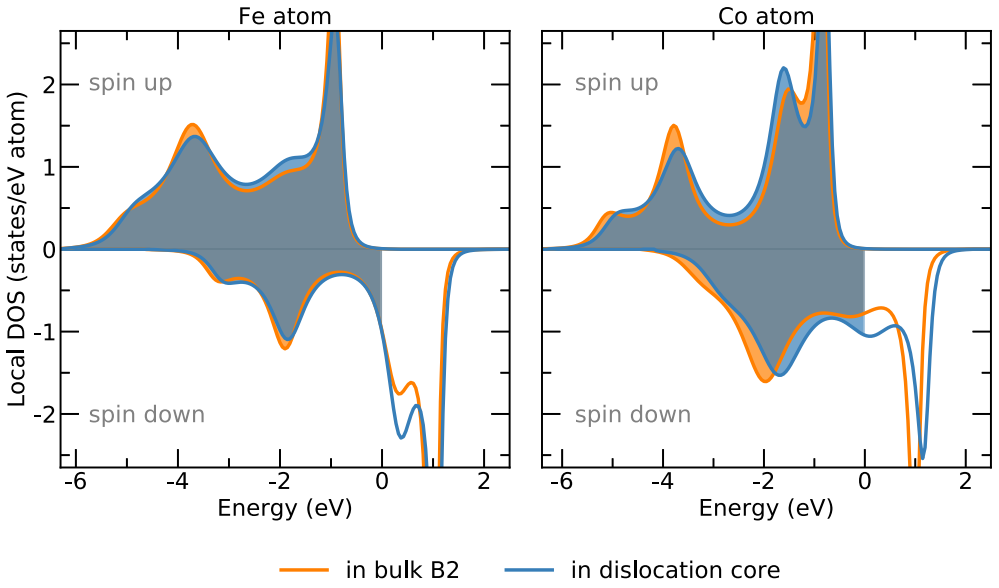

FIG. 6. Local density of states (DOS) of Fe and Co atoms in the dislocation core and bulk B2 FeCo computed with BOP.

(iv) Magnetic moments decrease in the cores; just as in disordered FeCo alloys [32].

(v) Dislocations alter the local DOS—and thus atomic interactions—in the cores.

(vi) Significant alterations in the local DOS for Co atoms in the core (unlike Fe atoms) are expected to increase band energy and, hence, the Peierls energy.

ACKNOWLEDGMENTS

We thank L. la Rosa and F. Maresca for their valuable comments on the manuscript. We acknowledge financial support from the International Max-Planck Research School SurMat and the Wilhelm and Günter Esser Foundation. The DFG supported part of this work within the DFG-ANR Project MAGIKID (No. 316673557).

[1] R. S. Sundar and S. C. Deevi, Soft magnetic FeCo alloys: Alloy development, processing, and properties, Int. Mat. Rev. **50**, 157 (2005).

[2] P. M. Anderson, J. P. Hirth, and J. Lothe, *Theory of Dislocations* (Cambridge University Press, Cambridge, 2017).

[3] N. Stoloff and R. Davies, The plastic deformation of ordered FeCo and Fe_3Al alloys, Acta Metall. **12**, 473 (1964).

[4] M. J. Marcinkowski and H. Chessin, Relationship between flow stress and atomic order in the FeCo alloy, Philos. Mag. A **10**, 837 (1964).

[5] L. Zhao and I. Baker, The effect of grain size and Fe:Co ratio on the room temperature yielding of FeCo, Acta Metall. Mater. **42**, 1953 (1994).

[6] E. George, A. Gubbi, I. Baker, and L. Robertson, Mechanical properties of soft magnetic FeCo alloys, Mater. Sci. Eng.: A **329-331**, 325 (2002).

[7] K. Sadananda and M. Marcinkowski, Dislocation behaviour in ordered alloys in the presence of frictional forces, J. Mater. Sci. **8**, 839 (1973).

[8] M. Marcinkowski and K. Sadananda, Effect of antiphase boundary energy on mutual cross slip of unlike dislocations, J. Appl. Phys. **45**, 2441 (1974).

[9] H. Gholizadeh and S. Hasani, *Ab-initio* calculation of the γ-surface and cleavage energy in the B2 FeCo intermetallic compound, Comput. Mater. Sci. **143**, 515 (2018).

[10] Y. Li, X. Cheng, W. Duan, and W. Qiang, Improved ductility by coupled motion of grain boundaries in nanocrystalline B2-FeCo alloys, Comput. Mater. Sci. **198**, 110703 (2021).

[11] M. Muralles, J. T. Oh, and Z. Chen, Molecular dynamics study of FeCo phase transitions and thermal properties based on an improved 2NN MEAM potential, J. Mater. Res. Technol. **19**, 1102 (2022).

[12] M. Muralles, J. Oh, and Z. Chen, Influence of V addition on the mechanical properties of FeCo alloys: A molecular dynamics study, Mater. **27**, 101670 (2023).

[13] W. Sigle, High-resolution electron microscopy and molecular dynamics study of the (a/2)[111] screw dislocation in molybdenum, Philos. Mag. A **79**, 1009 (1999).

[14] B. G. Mendis, Y. Mishin, C. S. Hartley, and K. J. Hemker, Use of the Nye tensor in analyzing HREM images of bcc screw dislocations, Philos. Mag. **86**, 4607 (2006).

[15] R. Gröger, K. J. Dudeck, P. D. Nellist, V. Vitek, P. B. Hirsch, and D. Cockayne, Effect of Eshelby twist on core structure of screw dislocations in molybdenum: Atomic structure and electron microscope image simulations, Philos. Mag. **91**, 2364 (2011).

[16] P. Hohenberg and W. Kohn, Inhomogeneous electron gas, Phys. Rev. **136**, B864 (1964).

[17] W. Kohn and L. J. Sham, Self-consistent equations including exchange and correlation effects, Phys. Rev. **140**, A1133 (1965).

[18] J. S. Koehler and F. Seitz, Proposed experiments for further study of the mechanism of plastic deformation, J. Appl. Mech. **14**, A217 (1947).

[19] A. P. Sutton, *Concepts of Materials Science* (Oxford University Press, Oxford, 2021).

[20] J. E. Gordon, *The New Science of Strong Materials* (Princeton University Press, Princeton, 2006), Vol. 58.

[21] M. Duesbery, V. Vitek, and D. K. Bowen, The effect of shear stress on the screw dislocation core structure in body-centred cubic lattices, Proc. R. Soc. London A **332**, 85 (1973).

[22] J. Christian, Some surprising features of the plastic deformation of body-centered cubic metals and alloys, Metall. Trans. A **14**, 1237 (1983).

[23] V. Vitek and V. Paidar, Chapter 87 - Non-Planar Dislocation Cores: A Ubiquitous Phenomenon Affecting Mechanical Properties of Crystalline Materials, in *A Tribute to F.R.N. Nabarro, Dislocations in Solids*, edited by J. P. Hirth (Elsevier, Amsterdam, Oxford, 2008), Vol. 14, pp. 439–514.

[24] D. Weygand, M. Mrovec, T. Hochrainer, and P. Gumbsch, Multiscale simulation of plasticity in bcc metals, Annu. Rev. Mater. Res. **45**, 369 (2015).

[25] C. Woodward and S. I. Rao, *Ab-initio* simulation of isolated screw dislocations in bcc Mo and Ta, Philos. Mag. A **81**, 1305 (2001).

[26] S. Ismail-Beigi and T. A. Arias, *Ab initio* study of screw dislocations in Mo and Ta: A new picture of plasticity in bcc transition metals, Phys. Rev. Lett. **84**, 1499 (2000).

[27] S. L. Frederiksen and K. W. Jacobsen, Density functional theory studies of screw dislocation core structures in bcc metals, Philos. Mag. **83**, 365 (2003).

[28] L. Dezerald, L. Ventelon, E. Clouet, C. Denoual, D. Rodney, and F. Willaime, *Ab initio* modeling of the two-dimensional energy landscape of screw dislocations in bcc transition metals, Phys. Rev. B **89**, 024104 (2014).

[29] C. R. Weinberger, G. J. Tucker, and S. M. Foiles, Peierls potential of screw dislocations in bcc transition metals: Predictions from density functional theory, Phys. Rev. B **87**, 054114 (2013).

[30] M. R. Gilbert and S. L. Dudarev, *Ab initio* multi-string Frenkel–Kontorova model for a b = a/2[111] screw dislocation in bcc iron, Philos. Mag. **90**, 1035 (2010).

[31] L. Romaner, C. Ambrosch-Draxl, and R. Pippan, Effect of rhenium on the dislocation core structure in tungsten, Phys. Rev. Lett. **104**, 195503 (2010).

[32] L. Romaner, V. Razumovskiy, and R. Pippan, Core polarity of screw dislocations in Fe–Co alloys, Philos. Mag. Lett. **94**, 334 (2014).

[33] O. von Goldbeck, Iron—cobalt Fe—Co, in *IRON—Binary Phase Diagrams* (Springer, Berlin, Heidelberg, 1982), pp. 27–31.

[34] A. Egorov, A. P. A. Subramanyam, Z. Yuan, R. Drautz, and T. Hammerschmidt, Magnetic bond-order potential for iron-cobalt alloys, Phys. Rev. Mater. **7**, 044403 (2023).

[35] Cores are visualized by a differential displacement [109] as implemented in the ATOMMAN package [122].

[36] P. Moine, J. Eymery, and P. Grosbras, The effects of short-range order and long-range order on the equilibrium configuration of superdislocations in Fe—Co: 2 at% V—Consequences on flow stress, Phys. Status Solidi (b) **46**, 177 (1971).

[37] M. Marcinkowski, The effect of atomic order on the mechanical properties of alloys with emphasis on feco, in *Order-Disorder Transformations in Alloys: Proceedings of the International Symposium on Order-Disorder Transformations in Alloys held 3–6 September 1973 in Tübingen, Germany* (Springer, Berlin, Heidelberg, New York, 1974), pp. 364–403.

[38] M. J. Marcinkowski, Theory and Direct Observation of Antiphase Boundaries and Dislocations in Superlattices, in *Electron Microscopy and Strength of Crystals*, edited by G. Thomas and J. Washburn (Interscience Publishers, New York, 1963), pp. 333–440.

[39] E. Clouet, *Ab initio* models of dislocations, in *Handbook of Materials Modeling: Methods: Theory and Modeling*, edited by W. Andreoni and S. Yip (Springer International Publishing, Cham, 2020), pp. 1503–1524.

[40] M. S. Daw and M. I. Baskes, Embedded-atom method: Derivation and application to impurities, surfaces, and other defects in metals, Phys. Rev. B **29**, 6443 (1984).

[41] M. I. Baskes, Modified embedded-atom potentials for cubic materials and impurities, Phys. Rev. B **46**, 2727 (1992).

[42] B.-J. Lee and M. I. Baskes, Second nearest-neighbor modified embedded-atom-method potential, Phys. Rev. B **62**, 8564 (2000).

[43] B.-J. Lee, M. Baskes, H. Kim, and Y. K. Cho, Second nearest-neighbor modified embedded atom method potentials for bcc transition metals, Phys. Rev. B **64**, 184102 (2001).

[44] V. Vitek, Core structure of screw dislocations in body-centred cubic metals: relation to symmetry and interatomic bonding, Philos. Mag. **84**, 415 (2004).

[45] D. Nguyen-Manh, V. Vitek, and A. Horsfield, Environmental dependence of bonding: A challenge for modelling of intermetallics and fusion materials, Prog. Mater. Sci. **52**, 255 (2007), Modelling electrons and atoms for materials science.

[46] R. J. Hawkins and J. Sanchez, Ferromagnetism and chemical ordering in cobalt-iron, J. Phys. F: Met. Phys. **18**, 767 (1988).

[47] I. A. Abrikosov, P. James, O. Eriksson, P. Söderlind, A. V. Ruban, H. L. Skriver, and B. Johansson, Magnetically induced crystal structure and phase stability in $Fe_{1-c}Co_c$, Phys. Rev. B **54**, 3380 (1996).

[48] M. Neumayer and M. Fähnle, Atomic defects in FeCo: Stabilization of the B2 structure by magnetism, Phys. Rev. B **64**, 132102 (2001).

[49] V. L. Deringer, M. A. Caro, and G. Csányi, Machine learning interatomic potentials as emerging tools for materials science, Adv. Mater. **31**, 1902765 (2019).

[50] Y. Mishin, Machine-learning interatomic potentials for materials science, Acta Mater. **214**, 116980 (2021).

[51] J. Behler and G. Csányi, Machine learning potentials for extended systems: a perspective, Eur. Phys. J. B **94**, 142 (2021).

[52] H. Kulik, T. Hammerschmidt, J. Schmidt, S. Botti, M. Marques, M. Boley, M. Scheffler, M. Todorović, P. Rinke, C. Oses *et al.*, Roadmap on machine learning in electronic structure, Electron. Struct. **4**, 023004 (2022).

[53] R. Freitas and Y. Cao, Machine-learning potentials for crystal defects, MRS Commun. **12**, 510 (2022).

[54] D. Dragoni, T. D. Daff, G. Csányi, and N. Marzari, Achieving DFT accuracy with a machine-learning interatomic potential: Thermomechanics and defects in bcc ferromagnetic iron, Phys. Rev. Mater. **2**, 013808 (2018).

[55] F. Maresca, D. Dragoni, G. Csányi, N. Marzari, and W. A. Curtin, Screw dislocation structure and mobility in body centered cubic Fe predicted by a Gaussian Approximation Potential, npj Comput. Mater. **4**, 69 (2018).

[56] H. Mori and T. Ozaki, Neural network atomic potential to investigate the dislocation dynamics in bcc iron, Phys. Rev. Mater. **4**, 040601 (2020).

[57] Y.-S. Lin, G. P. P. Pun, and Y. Mishin, Development of a physically-informed neural network interatomic potential for tantalum, Comput. Mater. Sci. **205**, 111180 (2022).

[58] M. Rinaldi, M. Mrovec, A. Bochkarev, Y. Lysogorskiy, and R. Drautz, Non-collinear magnetic atomic cluster expansion for iron, npj Comput. Mater. **10**, 12 (2024).

[59] R. Wang, X. Ma, L. Zhang, H. Wang, D. J. Srolovitz, T. Wen, and Z. Wu, Classical and machine learning interatomic potentials for bcc vanadium, Phys. Rev. Mater. **6**, 113603 (2022).

[60] L. Zhang, G. Csányi, E. van der Giessen, and F. Maresca, Efficiency, accuracy, and transferability of machine learning potentials: Application to dislocations and cracks in iron, Acta Mater. **270**, 119788 (2024).

[61] M. Eckhoff and J. Behler, High-dimensional neural network potentials for magnetic systems using spin-dependent atom-centered symmetry functions, npj Comput. Mater. **7**, 170 (2021).

[62] R. Drautz, Atomic cluster expansion of scalar, vectorial, and tensorial properties including magnetism and charge transfer, Phys. Rev. B **102**, 024104 (2020).

[63] I. Novikov, B. Grabowski, F. Körmann, and A. Shapeev, Magnetic moment tensor potentials for collinear spin-polarized materials reproduce different magnetic states of bcc Fe, npj Comput. Mater. **8**, 13 (2022).

[64] J. B. Chapman and P.-W. Ma, A machine-learned spin-lattice potential for dynamic simulations of defective magnetic iron, Sci. Rep. **12**, 22451 (2022).

[65] A. S. Kotykhov, K. Gubaev, M. Hodapp, C. Tantardini, A. V. Shapeev, and I. S. Novikov, Constrained DFT-based magnetic machine-learning potentials for magnetic alloys: a case study of Fe–Al, Sci. Rep. **13**, 19728 (2023).

[66] Z. Yuan, Z. Xu, H. Li, X. Cheng, H. Tao, Z. Tang, Z. Zhou, W. Duan, and Y. Xu, Equivariant neural network force fields for magnetic materials, Quant. Front. **3**, 8 (2024).

[67] R. Drautz and D. G. Pettifor, Valence-dependent analytic bond-order potential for transition metals, Phys. Rev. B **74**, 174117 (2006).

[68] R. Drautz and D. G. Pettifor, Valence-dependent analytic bond-order potential for magnetic transition metals, Phys. Rev. B **84**, 214114 (2011).

[69] J. F. Drain, R. Drautz, and D. G. Pettifor, Magnetic analytic bond-order potential for modeling the different phases of Mn at zero kelvin, Phys. Rev. B **89**, 134102 (2014).

[70] M. Ford, R. Drautz, T. Hammerschmidt, and D. G. Pettifor, Convergence of an analytic bond-order potential for collinear magnetism in Fe, Modell. Simul. Mater. Sci. Eng. **22**, 034005 (2014).

[71] M. Čák, T. Hammerschmidt, J. Rogal, V. Vitek, and R. Drautz, Analytic bond-order potentials for the bcc refractory metals Nb, Ta, Mo and W, J. Phys.: Condens. Matter **26**, 195501 (2014).

[72] A. Ferrari, M. Schröder, Y. Lysogorskiy, J. Rogal, M. Mrovec, and R. Drautz, Phase transitions in titanium with an analytic bond-order potential, Modell. Simul. Mater. Sci. Eng. **27**, 085008 (2019).

[73] A. P. A. Subramanyam, J. Jenke, A. N. Ladines, R. Drautz, and T. Hammerschmidt, Parametrization protocol and refinement strategies for accurate and transferable analytic bond-order potentials: Application to Re, Phys. Rev. Mater. **8**, 013803 (2024).

[74] M. Mrovec, R. Gröger, A. G. Bailey, D. Nguyen-Manh, C. Elsässer, and V. Vitek, Bond-order potential for simulations of extended defects in tungsten, Phys. Rev. B **75**, 104119 (2007).

[75] M. Mrovec, D. Nguyen-Manh, D. G. Pettifor, and V. Vitek, Bond-order potential for molybdenum: Application to dislocation behavior, Phys. Rev. B **69**, 094115 (2004).

[76] M. Mrovec, D. Nguyen-Manh, C. Elsässer, and P. Gumbsch, Magnetic bond-order potential for iron, Phys. Rev. Lett. **106**, 246402 (2011).

[77] G. Kresse and J. Hafner, *Ab initio* molecular dynamics for liquid metals, Phys. Rev. B **47**, 558 (1993).

[78] G. Kresse and J. Hafner, *Ab initio* molecular-dynamics simulation of the liquid-metal–amorphous-semiconductor transition in germanium, Phys. Rev. B **49**, 14251 (1994).

[79] G. Kresse and J. Furthmüller, Efficiency of *ab-initio* total energy calculations for metals and semiconductors using a plane-wave basis set, Comput. Mater. Sci. **6**, 15 (1996).

[80] G. Kresse and D. Joubert, From ultrasoft pseudopotentials to the projector augmented-wave method, Phys. Rev. B **59**, 1758 (1999).

[81] J. P. Perdew, K. Burke, and M. Ernzerhof, Generalized gradient approximation made simple, Phys. Rev. Lett. **77**, 3865 (1996).

[82] H. J. Monkhorst and J. D. Pack, Special points for Brillouin-zone integrations, Phys. Rev. B **13**, 5188 (1976).

[83] T. Hammerschmidt, B. Seiser, M. Ford, A. Ladines, S. Schreiber, N. Wang, J. Jenke, Y. Lysogorskiy, C. Teijeiro, M. Mrovec, M. Cak, E. Margine, D. Pettifor, and R. Drautz, BOPFOX program for tight-binding and analytic bond-order potential calculations, Comput. Phys. Commun. **235**, 221 (2019).

[84] A. P. Thompson, H. M. Aktulga, R. Berger, D. S. Bolintineanu, W. M. Brown, P. S. Crozier, P. J. in 't Veld, A. Kohlmeyer, S. G. Moore, T. D. Nguyen, R. Shan, M. J. Stevens, J. Tranchida, C. Trott, and S. J. Plimpton, LAMMPS - a flexible simulation tool for particle-based materials modeling at the atomic, meso, and continuum scales, Comput. Phys. Commun. **271**, 108171 (2022).

[85] A. H. Larsen, J. J. Mortensen, J. Blomqvist, I. E. Castelli, R. Christensen, M. Dułak, J. Friis, M. N. Groves, B. Hammer, C. Hargus *et al.*, The atomic simulation environment—a Python library for working with atoms, J. Phys.: Condens. Matter **29**, 273002 (2017).

[86] E. Bitzek, P. Koskinen, F. Gähler, M. Moseler, and P. Gumbsch, Structural relaxation made simple, Phys. Rev. Lett. **97**, 170201 (2006).

[87] V. Vítek, Intrinsic stacking faults in body-centred cubic crystals, Philos. Mag. A **18**, 773 (1968).

[88] See Supplemental Material at http://link.aps.org/supplemental/10.1103/PhysRevMaterials.8.093604 for details and results of modeling the [111] screw superdislocation in B2 FeCo with BOP.

[89] L. Ventelon and F. Willaime, Core structure and Peierls potential of screw dislocations in α-Fe from first principles: Cluster

versus dipole approaches, J. Comput.-Aided Mater. Des. **14**, 85 (2007).
[90] E. Clouet, L. Ventelon, and F. Willaime, Dislocation core energies and core fields from first principles, Phys. Rev. Lett. **102**, 055502 (2009).
[91] E. Clouet, BABEL package, version 10.7.
[92] E. Clouet, B. Bienvenu, L. Dezerald, and D. Rodney, Screw dislocations in BCC transition metals: from *ab initio* modeling to yield criterion, Comptes Rendus. Physique **22**, 83 (2021).
[93] A. Kraych, E. Clouet, L. Dezerald, L. Ventelon, F. Willaime, and D. Rodney, Non-glide effects and dislocation core fields in bcc metals, npj Comput. Mater. **5**, 109 (2019).
[94] To distinguish dislocation cores, the atoms are colored according to common neighbor analysts [123] implemented in the OVITO package [124] (We also used a Polyhedral template matching [125] to visualize superdislocation cores, as shown in the Supplemental Material [88]).
[95] M. Yamaguchi, Y. Umakoshi, T. Yamane, Y. Minonishi, and S. Morozumi, Slip systems in an Fe-54 At. % Co alloy, Scr. Metall. **16**, 607 (1982).
[96] W.-M. Choi, Y. Kim, D. Seol, and B.-J. Lee, Modified embedded-atom method interatomic potentials for the Co-Cr, Co-Fe, Co-Mn, Cr-Mn and Mn-Ni binary systems, Comput. Mater. Sci. **130**, 121 (2017).
[97] V. Paidar and M. Čák, Three types of dislocation core structure in B2 alloys, Intermetallics **73**, 21 (2016).
[98] M. Duesbery and V. Vitek, Plastic anisotropy in b.c.c. transition metals, Acta Mater. **46**, 1481 (1998).
[99] B. Bienvenu, C. C. Fu, and E. Clouet, Impact of magnetism on screw dislocations in body-centered cubic chromium, Acta Mater. **200**, 570 (2020).
[100] B. Bienvenu, C. C. Fu, and E. Clouet, Interplay between magnetic excitations and plasticity in body-centered cubic chromium, Phys. Rev. B **107**, 134105 (2023).
[101] X. Xu, X. Zhang, A. Ruban, S. Schmauder, and B. Grabowski, Strong impact of spin fluctuations on the antiphase boundaries of weak itinerant ferromagnetic Ni_3Al, Acta Mater. **255**, 118986 (2023).
[102] R. Sun and D. D. Johnson, Stability maps to predict anomalous ductility in B2 materials, Phys. Rev. B **87**, 104107 (2013).
[103] We adopted the Voigt-Reuss-Hill shear modulus, which fits experimental values well [126].
[104] A. Jain, S. P. Ong, G. Hautier, W. Chen, W. D. Richards, S. Dacek, S. Cholia, D. Gunter, D. Skinner, G. Ceder, and K. A. Persson, The Materials Project: A materials genome approach to accelerating materials innovation, APL Mater. **1**, 011002 (2013).
[105] C. L. Fu and M. Krčmar, First-principles study of the structural, defect, and mechanical properties of B2 FeCo alloys, Phys. Rev. B **74**, 174108 (2006).
[106] O. Belousov and N. Palii, Concentration and temperature dependences of the elastic properties of quenched Fe-Co and FeCo-2V alloys, Russ. Metall. **2009**, 41 (2009).
[107] Differential displacement, Nye tensor, and magnetic moments are visualized with the ATOMMAN package [122].
[108] The pale red dot at the right edge results from numerical extrapolation to create a smooth plot from discrete values of the Nye tensor and does not impart significant meaning.
[109] V. Vítek, R. C. Perrin, and D. K. Bowen, The core structure of 1/2(111) screw dislocations in b.c.c. crystals, Philos. Mag. A **21**, 1049 (1970).
[110] J. Nye, Some geometrical relations in dislocated crystals, Acta Metall. **1**, 153 (1953).
[111] C. Hartley and Y. Mishin, Characterization and visualization of the lattice misfit associated with dislocation cores, Acta Mater. **53**, 1313 (2005).
[112] C. S. Hartley and Y. Mishin, Representation of dislocation cores using Nye tensor distributions, Mater. Sci. Eng.: A **400-401**, 18 (2005).
[113] L. Casillas-Trujillo and B. Alling, Configurational thermodynamics of a $1/2\langle 111\rangle$ screw dislocation core in Mo–W solid solutions using cluster expansion, J. Appl. Phys. **128**, 045114 (2020).
[114] H. Li, S. Wurster, C. Motz, L. Romaner, C. Ambrosch-Draxl, and R. Pippan, Dislocation-core symmetry and slip planes in tungsten alloys: *Ab initio* calculations and microcantilever bending experiments, Acta Mater. **60**, 748 (2012).
[115] G. D. Samolyuk, Y. Osetsky, and R. Stoller, The influence of transition metal solutes on the dislocation core structure and values of the Peierls stress and barrier in tungsten, J. Phys.: Condens. Matter **25**, 025403 (2013).
[116] R. Wang, L. Zhu, S. Pattamatta, D. J. Srolovitz, and Z. Wu, The taming of the screw: Dislocation cores in bcc metals and alloys, Mater. Today (2024), doi: 10.1016/j.mattod.2024.07.009.
[117] M. Rahaman, A. V. Ruban, A. Mookerjee, and B. Johansson, Magnetic state effect upon the order-disorder phase transition in Fe-Co alloys: A first-principles study, Phys. Rev. B **83**, 054202 (2011).
[118] G. Liu, D. Nguyen-Manh, B.-G. Liu, and D. G. Pettifor, Magnetic properties of point defects in iron within the tight-binding-bond Stoner model, Phys. Rev. B **71**, 174115 (2005).
[119] L. Ventelon, F. Willaime, E. Clouet, and D. Rodney, *Ab initio* investigation of the Peierls potential of screw dislocations in bcc Fe and W, Acta Mater. **61**, 3973 (2013).
[120] K. Odbadrakh, A. Rusanu, G. M. Stocks, G. D. Samolyuk, M. Eisenbach, Y. Wang, and D. M. Nicholson, Calculated electronic and magnetic structure of screw dislocations in alpha iron, J. Appl. Phys. **109**, 07E159 (2011).
[121] L. Casillas-Trujillo, D. Gambino, L. Ventelon, and B. Alling, Screw dislocation core structure in the paramagnetic state of bcc iron from first-principles calculations, Phys. Rev. B **102**, 094420 (2020).
[122] NIST, ATOMMAN: Atomistic manipulation toolkit, https://www.ctcms.nist.gov/potentials/atomman/.
[123] J. D. Honeycutt and H. C. Andersen, Molecular dynamics study of melting and freezing of small Lennard-Jones clusters, J. Phys. Chem. **91**, 4950 (1987).
[124] A. Stukowski, Visualization and analysis of atomistic simulation data with OVITO–the Open Visualization Tool, Modell. Simul. Mater. Sci. Eng. **18**, 015012 (2010).
[125] P. M. Larsen, S. Schmidt, and J. Schiøtz, Robust structural identification via polyhedral template matching, Modell. Simul. Mater. Sci. Eng. **24**, 055007 (2016).
[126] D. Chung and W. Buessem, The Voigt-Reuss-Hill approximation and elastic moduli of polycrystalline MgO, CaF2, β-ZnS, ZnSe, and CdTe, J. Appl. Phys. **38**, 2535 (1967).